Viscous fingering of a miscible reactive $A + B \rightarrow C$ interface: a linear stability analysis

S. H. HEJAZI[1], P. M. J. TREVELYAN[2], J. AZAIEZ[1] AND A. DE WIT[2]†

[1]Department of Chemical and Petroleum Engineering, University of Calgary,
Calgary, Alberta, Canada T2N 1N4
[2]Nonlinear Physical Chemistry Unit, Faculté des Sciences,
Université Libre de Bruxelles (ULB), CP 231, 1050 Brussels, Belgium

When one solution of reactant A is displacing another miscible solution of reactant B, a miscible product C can be generated in the contact zone if a simple $A + B \rightarrow C$ chemical reaction takes place. Depending on the relative effect of A, B and C on the viscosity, different viscous fingering (VF) instabilities can be observed. In this context, a linear stability analysis of this reaction–diffusion–convection problem under the quasi-steady-state approximation is performed to classify the various possible instability scenarios. To do so, we determine the criteria for an instability, obtain dispersion curves both at initial contact time using an analytical implicit solution and at later times via numerical stability analysis. Along with recovering known results for non-reactive systems where the displacement of a more viscous fluid by a less viscous one leads to a VF instability, it is found that in the presence of a chemical reaction, injecting a more viscous fluid into a less viscous fluid can also lead to instabilities. This occurs when the chemical reaction leads to the build up of non-monotonic viscosity profiles. Various instability scenarios are classified in a parameter plane spanned by R_b and R_c representing the log-mobility ratios of the viscosities of the B and C solution respectively with respect to that of the injected solution of A. A parametric study of the influence on stability of the Damköhler number and of the time elapsed after contact of the two reactive solutions is also conducted.

1. Introduction

Reactive systems are able to trigger hydrodynamic flows as soon as the chemical reaction changes the physical property of the fluid such as its density, surface tension or viscosity. In the case of viscosity in particular, a viscous fingering (VF) instability, occurring in a porous medium when a given fluid displaces another more viscous fluid Homsy (1987), can be triggered or influenced by a chemical reaction changing the viscosity of the solution. Experimental evidences and theoretical studies of such chemically influenced viscous fingering have been obtained for reactions changing the permeability of the porous matrix by dissolution (Chadam *et al.* 1986; Wei & Ortoleva 1990) or precipitation (Nagatsu *et al.* 2008). In the case of immiscible flows, this instability, known as the Saffman–Taylor instability, can also be modified by reactions that change the surface tension at the fluid interface (Jahoda &

† Email address for correspondence: adewit@ulb.ac.be

Hornof 2000; Fernandez & Homsy 2003). Several works have moreover addressed theoretically the coupling between VF and autocatalytic reactions (De Wit & Homsy 1999*a*, 1999*b*; Swernath & Pushpavanam 2007, 2008; Ghesmat & Azaiez 2009) without however corresponding experimental confirmations as autocatalytic reactions are more prone to change density rather than viscosity (De Wit 2001; De Wit *et al.* 2003). In the context of chromatographic applications, adsorption–desorption phenomena have also been shown to influence VF patterns (Mishra, Martin & De Wit 2007).

More recently, experiments demonstrating the influence of a simple $A + B \rightarrow C$ chemical reaction on the properties of viscous fingering between miscible solutions of initially separated reactants A and B have rejuvenated the interest for a theoretical classification of the possible VF instability scenarios for miscible reactive fluids. Indeed, Nagatsu *et al.* (2007) have first shown that depending on the reactants at hand, the reaction can either increase or decrease the viscosity of the solution, which has important effects on the width and scalings of the fingers in time. They have also tuned the chemistry to analyse fingering at both large and moderate Damköhler numbers, i.e. at respectively strong and moderate effects of chemistry on the flow (Nagatsu *et al.* 2007, 2009). In parallel, Podgorski *et al.* (2007) have also examined experimentally purely chemically driven viscous fingering in a system where the two A and B reactant solutions have the same viscosity but the product C is more viscous. Strikingly, the fingering patterns differ depending on whether A is injected into B or vice versa. The VF properties of such an $A + B \rightarrow C$ reactive system have been studied numerically in the case where the reactants have the same viscosity and the product is more viscous (Gérard & De Wit 2009). It has been shown that VF patterns can indeed be different depending on whether A displaces B or vice versa, when the diffusion coefficients or initial concentrations of the two reactants are different. A more recent study by Hejazi & Azaiez (2010) examined flows where the reactants and the chemical product all have different viscosities. The study analysed the effects of the viscosity ratios as well as of the Péclet number on the development of the VF.

When considering miscible solutions involving three key chemical species A, B and C related by a simple bimolecular reaction $A + B \rightarrow C$, it is easy to understand that fingering properties will depend on the relative values of the viscosities μ_A, μ_B and μ_C of the pure solutions of the three chemicals. The present study focuses on the case where A is injected into B, i.e. the porous medium is initially filled with the reactant solution B which is displaced by a solution of A injected at a constant speed U. If the reactant A has a viscosity larger than or equal to that of the reactant B, then the non-reactive system is stable with regard to VF. However, for reactive systems, fingering can occur if the product C has a viscosity different from that of the reactants. If, on the contrary, the non-reactive system is already genuinely unstable because B is more viscous than A, then the properties of the reactive fingering instability can nevertheless also be affected by the generation of a product of different viscosity.

To gain insight into the way a chemical reaction may affect the stability of the system with regard to a VF instability, a reaction–diffusion–convection (RDC) model coupling Darcy's law to evolution equations for the concentrations of species A, B and C is used. The viscosity, non-dimensionalized by μ_A, depends on the concentration of B and C through two log-mobility ratios R_b and R_c quantifying respectively the ratio between the viscosity of the reactant B and product C and that of the reactant A. A peculiarity of the stability of such systems is that the base state of the problem is
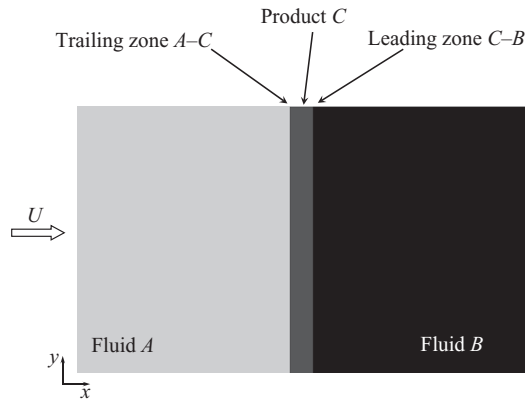
FIGURE 1. Schematic of the displacement process with chemical reaction.

time dependent as the reaction proceeds and more and more product C is generated in the course of time. The viscosity profile varies therefore in time and the related stability can thus change as time goes by. A linear stability analysis (LSA) of the time-dependent base state of the model is conducted both analytically at time $t = 0$ and numerically for later times using a quasi-steady-state approximation. A parametric study is performed in terms of the log-mobility ratios R_b and R_c as well as of the Damköhler number of the problem.

The paper is organized as follows. In §2, the RDC model of the problem is introduced and the relevant dimensionless parameters are defined. The base-state viscosity profile is discussed in terms of the parameters of the problem. Section 3 introduces the linear stability analysis equations that are solved analytically at $t = 0$ in §4 and numerically at later times in §5. The discussions and conclusions are given in §6.

2. Mathematical model

2.1. *Formulation of the problem*

We consider a two-dimensional porous medium or equivalently a horizontal Hele-Shaw cell having a gap width sufficiently small with regard to the other two dimensions so that the flow evolution can be considered to be governed by two-dimensional Darcy's law. A schematic of the flow geometry is shown in figure 1. Initially the cell is filled with a solution of B having a viscosity μ_B. A miscible solution of A of viscosity μ_A is injected from the left side at a uniform velocity U along the x direction, the coordinate y being aligned along the perpendicular direction. It is assumed throughout that A and B have the same initial concentration, a_0. The following reaction occurs as soon as species A and B are in contact:

$$A + B \rightarrow C. \tag{2.1}$$

The chemical product C has a viscosity μ_C that, in general, will be assumed to be different from that of either reactants. The flow system is modelled using the

continuity equation, Darcy's law and three RDC equations, namely

$$\nabla \cdot \boldsymbol{u} = 0, \tag{2.2}$$

$$\boldsymbol{u} = -\frac{\kappa}{\mu}\nabla p, \tag{2.3}$$

$$\frac{\partial A}{\partial t} + \boldsymbol{u} \cdot \nabla A = D_A \nabla^2 A - kAB, \tag{2.4}$$

$$\frac{\partial B}{\partial t} + \boldsymbol{u} \cdot \nabla B = D_B \nabla^2 B - kAB, \tag{2.5}$$

$$\frac{\partial C}{\partial t} + \boldsymbol{u} \cdot \nabla C = D_C \nabla^2 C + kAB, \tag{2.6}$$

where $\boldsymbol{u} = (u, v)$ stands for the two-dimensional velocity vector, μ is the viscosity, κ is the medium permeability and p is the pressure. Note that A, B and C represent the dimensional concentrations of the two reactants and product, respectively, while D_A, D_B and D_C are their corresponding diffusion coefficients and k is the reaction constant. It will be assumed that all species involved have the same diffusion coefficient, i.e. $D_A = D_B = D_C = D$.

Formally the initial conditions are

$$u = U, \quad v = 0, \quad A = \begin{cases} a_0 & x < 0 \\ 0 & x > 0 \end{cases}, \quad B = \begin{cases} 0 & x < 0 \\ a_0 & x > 0 \end{cases} \quad \text{and} \quad C = 0.$$

For simplicity, the domain length is assumed infinite, which prevents the introduction of this length as an additional parameter in the problem.

In general, $\mu = \mu(A, B, C)$, and so we define explicitly $\mu_A = \mu(a_0, 0, 0)$, $\mu_B = \mu(0, a_0, 0)$ and $\mu_C = \mu(0, 0, a_0)$; thus, each constant represents the viscosity of the fluid when only one species is present at the concentration a_0. The exact dependence of the viscosity on concentrations B and C still needs to be specified. Following earlier studies (Tan & Homsy 1986; De Wit & Homsy 1999a, 1999b; Azaiez & Singh 2002; Gérard & De Wit 2009), an exponential dependence is adopted. The logarithm of the viscosity is thus taken to be a linear combination of the concentrations. Hence, without loss of generality, we can consider $\mu = \mu_A \mu(B, C)$ as all of the species diffuse at the same rate and we have equal initial concentrations of A and B. Therefore, one can write

$$\mu = \mu_A \, e^{(R_b B + R_c C)/a_0}, \tag{2.7}$$

where R_b and R_c are the log-mobility ratios between the viscosity of pure solutions at concentration a_0 defined as

$$R_b = \ln\left(\frac{\mu_B}{\mu_A}\right) \quad \text{and} \quad R_c = \ln\left(\frac{\mu_C}{\mu_A}\right). \tag{2.8}$$

Occasionally and with a slight terminology abuse, the log-mobility ratios will be referred to as simply the mobility ratios or viscosity ratios.

2.2. Dimensionless equations

In what follows, the flow will be examined in a Lagrangian reference frame moving with the average injection velocity U, i.e. we make the transformation

$$\hat{\boldsymbol{u}} = \boldsymbol{u} - U\hat{\boldsymbol{i}}, \tag{2.9}$$

where $\hat{\boldsymbol{i}}$ is the unit vector along x. The resulting system of equations is non-dimensionalized using the injection velocity U, diffusive length scale D/U, time D/U^2,

viscosity μ_A, pressure $\mu_A D/\kappa$ and concentration a_0. The following dimensionless equations are obtained:

$$\nabla \cdot \boldsymbol{u} = 0, \tag{2.10}$$

$$\boldsymbol{u} + \boldsymbol{i} = -\frac{1}{\mu}\nabla p, \tag{2.11}$$

$$\frac{\partial A}{\partial t} + \boldsymbol{u} \cdot \nabla A = \nabla^2 A - D_a AB, \tag{2.12}$$

$$\frac{\partial B}{\partial t} + \boldsymbol{u} \cdot \nabla B = \nabla^2 B - D_a AB, \tag{2.13}$$

$$\frac{\partial C}{\partial t} + \boldsymbol{u} \cdot \nabla C = \nabla^2 C + D_a AB, \tag{2.14}$$

$$\mu = e^{R_b B + R_c C}. \tag{2.15}$$

The Damköhler number $D_a = ka_0 D/U^2$ represents the ratio between the characteristic hydrodynamic time scale $\tau_h = D/U^2$ and the chemical time scale $\tau_c = 1/[ka_0]$.

2.3. *Base-state viscosity profiles of the reactive system*

In order to predict the influence of the chemical reaction on the stability of the system, let us first characterize the base state of the underlying reaction–diffusion (RD) dynamics.

In the absence of any transverse instabilities, there is no disturbance to the flow and the dynamics are one-dimensional. The system (2.10)–(2.15) admits a base-state solution corresponding to $u_0 = v_0 = 0$, where the base-state concentrations $A_0(x,t)$, $B_0(x,t)$ and $C_0(x,t)$ are solutions of the following RD equations:

$$\frac{\partial A_0}{\partial t} = \frac{\partial^2 A_0}{\partial x^2} - D_a A_0 B_0, \tag{2.16}$$

$$\frac{\partial B_0}{\partial t} = \frac{\partial^2 B_0}{\partial x^2} - D_a A_0 B_0, \tag{2.17}$$

$$\frac{\partial C_0}{\partial t} = \frac{\partial^2 C_0}{\partial x^2} + D_a A_0 B_0. \tag{2.18}$$

The appropriate linear combination of these equations leads to

$$\frac{\partial (A_0 + B_0 + 2C_0)}{\partial t} - \frac{\partial^2 (A_0 + B_0 + 2C_0)}{\partial x^2} = 0. \tag{2.19}$$

Given the initial and boundary conditions of the problem, the only possible solution is $A_0 + B_0 + 2C_0 = 1$. There is no exact analytic solution for the above set of base-state equations. It is however known that, when the two reactants have the same initial concentrations and diffusion coefficients as it is the case here, the reaction front defined as the region where the concentration of the chemical product is maximum remains at the location of initial contact between the two reactants (Gálfi & Rácz 1988; Jiang & Ebner 1990). In the moving reference frame, this front is at $x = 0$. On the basis of the asymptotic large time concentration profiles (Gálfi & Rácz 1988) and (2.15), the base-state viscosity profile is

$$\mu_0(x,t) = e^{R_b B_0(x,t) + R_c C_0(x,t)}. \tag{2.20}$$

Figure 2 shows the logarithm of the viscosity profiles as a function of the self-similar dimensionless variable $\eta = x/2\sqrt{t}$ for asymptotic large times. Two situations have to be distinguished depending on whether R_b is positive or negative. For $R_b > 0$, the
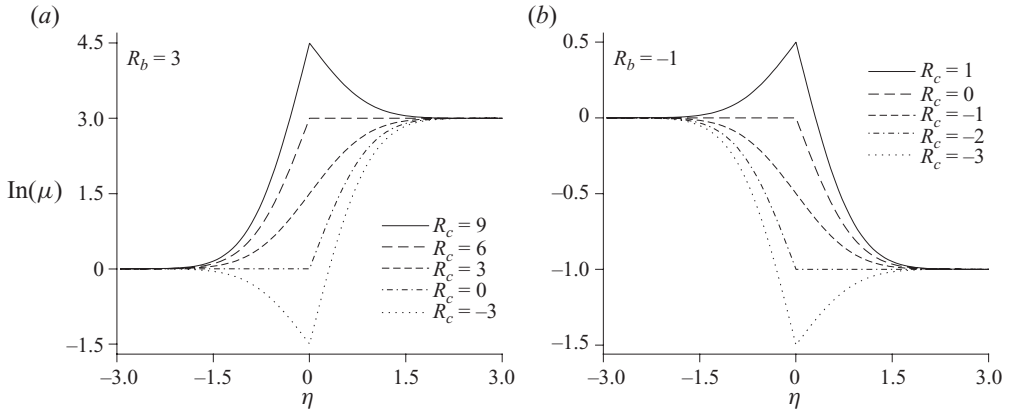
FIGURE 2. Log–viscosity profiles as a function of the self-similar variable η for asymptotic long-time concentration profiles ($t \to \infty$) for (*a*) $R_b = 3$, (*b*) $R_b = -1$ and various R_c.

system is genuinely unstable as the displacing reactant A is less viscous than the displaced reactant B (figure 2*a*). On the contrary, if $R_b < 0$, the non-reactive system is stable as the viscosity μ_A of the displacing solution of A is larger than that of the displaced solution of B (figure 2*b*). In both cases, the chemical reaction, by producing a product C of different viscosity, modifies the non-reactive viscosity profile except in the special case where $R_b = R_c$, i.e. when $\mu_B = \mu_c$. Depending on the relative value of R_c and R_b, the viscosity profile can remain monotonically increasing or decreasing or features an extremum due to a non-monotonic spatial variation.

Note that as all three species A, B and C diffuse, react and mix, it may be misleading to talk about a front between the A and C chemicals or between C and B. However, a close inspection of figure 2 shows (and this is especially visible on the non-monotonic viscosity profiles) that $\mu(\eta)$ varies differently depending on whether $\eta < 0$ or $\eta > 0$. It is therefore useful to introduce the notion of a 'trailing zone' defined as the zone for which $\eta < 0$, i.e. the zone between the solution of A and the location of the maximum production of C. Similarly, a 'leading zone' will be defined as the zone where $\eta > 0$, i.e. the zone where the location of the maximum production of C displaces the reactant B. These regions are schematically represented in figure 1. In addition, one can define $R_{AC} = \ln(\mu)|_{\eta=0} \equiv R_c/2$ and $R_{CB} = R_b - \ln(\mu)|_{\eta=0} \equiv R_b - R_c/2$ with $R_{AC} + R_{CB} = R_b$, where μ is constructed using large time asymptotic concentration profiles as in figure 2. These definitions determine the viscosity jumps between the pure reactant solutions and the reaction zone.

2.4. *Monotonic versus non-monotonic viscosity profiles*

Let us determine the location of monotonic versus non-monotonic viscosity profiles in the (R_b, R_c) plane and look at the values of the relative viscosity jumps R_{AC} and R_{CB} in each case. This classification follows the reasoning of Rongy, Trevelyan & De Wit (2008), who have proposed a somewhat similar classification for a reactive system in a horizontal layer in the case of buoyancy-driven convection.

The gradient of the base-state viscosity profile is obtained using (2.20) and the relationship $C_0 = (1 - A_0 - B_0)/2$ as

$$\frac{\partial \mu_0}{\partial x} = \mu_0 \left[\frac{R_c}{2} \left(-\frac{\partial A_0}{\partial x} \right) + \left(R_b - \frac{R_c}{2} \right) \frac{\partial B_0}{\partial x} \right]. \tag{2.21}$$
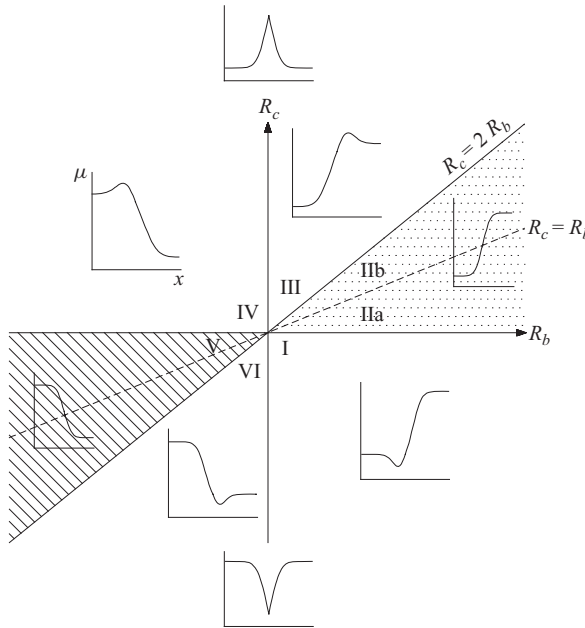
FIGURE 3. Large time asymptotic viscosity profiles in the (R_b, R_c) parameter plane.

Because the concentration profiles A_0 and B_0 are uniformly decreasing and increasing respectively, both $-\partial A_0/\partial x$ and $\partial B_0/\partial x$ are positive. A monotonic profile will thus occur when $R_c(R_b - R_c/2) > 0$, i.e. if $0 < R_c/2 < R_b$ (monotonic increase) or $R_b < R_c/2 < 0$ (monotonic decrease). The lines $R_c = 0$ and $R_c = 2R_b$ delimit therefore the location in the parameter space for which monotonic viscosity profiles are encountered (see shaded zones in figure 3). The profile exhibits an extremum whenever $\partial \mu_0/\partial x = 0$ somewhere along x which is obtained when $R_c(R_b - R_c/2) < 0$. In that case, either the trailing or leading zone is destabilizing. The flow is then expected to be unstable in the case of the monotonically increasing and non-monotonic viscosity profiles but stable in the case of the monotonically decreasing profiles. In this sense, the present study bears some similarities with earlier ones dealing with non-monotonic viscosity profiles (Manickam & Homsy 1993; Loggia *et al.* 1995; Loggia, Salin & Yortsos 1998; Pankiewitz & Meiburg 1999; De Wit, Bertho & Martin 2005; Schafroth, Goyal & Meiburg 2007). However, there is a fundamental difference arising from the important role of chemistry. As shall be seen later, along with the viscosity gradients, chemistry plays an important role and modifies the development of the instability in time for both monotonic and non-monotonic viscosity profiles.

   Figure 3 summarizes these results in the (R_b, R_c) plane. Insets of the viscosity profiles are shown. The shaded areas feature monotonic profiles with area V representing the stable case of a monotonically decreasing viscosity. The y-axis ($R_b = 0$) corresponds to the case where both reactants A and B have the same viscosity and the non-reactive flow is neutrally stable. The only unconditionally stable situation in that case is when $R_c = 0$ which corresponds to a constant and uniform viscosity in the whole system. As soon as $R_c \neq 0$ for $R_b = 0$, the product will have a viscosity different from that of the reactants and the viscosity profile presents an extremum, therefore triggering an instability. This case has recently been studied numerically in the nonlinear regime in the case $R_c > 0$ (Gérard & De Wit 2009).

The special case where the product C has the same viscosity as that of the reactant B corresponds to the dashed line $R_c = R_b$. The viscosity profile is then antisymmetric. The situation is therefore exactly analogous to that of a non-reactive displacement.

The x-axis ($R_c = 0$) represents a flow where the chemical product C has the same viscosity as the reactant A, implying a neutrally stable trailing zone (see figure 2). The viscosity profiles for this case are similar to those shown in the contiguous shaded areas, i.e. they do not have an extremum. However, as shown in figure 2 for both $R_c = 0$ cases, the viscosity profile of this reactive case is different from that with $R_c = R_b$. In particular, it has a larger viscosity gradient as now the same viscosity difference between A and B is confined to the leading zone only ($R_{CB} = R_b$). The reactive system is then expected to remain stable for $R_b < 0$ when the viscosity is monotonously decreasing and to be more unstable than its non-reactive equivalent for $R_b > 0$. Intuitively, a symmetric situation could be expected for the special case $R_c = 2R_b$, where now the same viscosity difference is concentrated on the trailing zone ($R_{AC} = R_b$) as seen in figure 2. However, as shown below, the cases $R_c = 0$ ($R_{AC} = 0$) and $R_c = 2R_b$ ($R_{CB} = 0$) are actually not similar.

Outside the dashed areas, the viscosity profiles are non-monotonic and the chemical reaction has then certainly an influence on the stability of the system. Before presenting a detailed analysis of this issue, we should note that intuitively, from figure 3, the flow is always unstable if the initial front between the two reactants is unstable (right part of the plane; $R_b > 0$). On the other hand, if the initial front is stable, then the flow may be stable or unstable (left part of the plane; $R_b \leqslant 0$).

Let us now proceed with the linear stability analysis that will allow us to gain more insight into the problem and check the above expectations.

3. Linear stability analysis

3.1. *Linearized equations*

In order to conduct the stability analysis, all dependent functions are expressed as the sum of the base-state solution and a perturbation:

$$\left.\begin{array}{l} A(x, y, t) = A_0(x, t) + A'(x, y, t), \\ B(x, y, t) = B_0(x, t) + B'(x, y, t), \\ C(x, y, t) = C_0(x, t) + C'(x, y, t), \\ p(x, y, t) = p_0(x, t) + p'(x, y, t), \\ \mu(x, y, t) = \mu_0(x, t) + \mu'(x, y, t), \\ u(x, y, t) = u'(x, y, t), \\ v(x, y, t) = v'(x, y, t), \end{array}\right\} \tag{3.1}$$

where primed terms represent small disturbances from the base states. Inserting the above expressions in (2.12)–(2.15) and linearizing them leads to

$$\frac{\partial A'}{\partial t} + u' \frac{\partial A_0}{\partial x} = \left(\frac{\partial^2}{\partial x^2} + \frac{\partial^2}{\partial y^2} \right) A' - D_a(A'B_0 + A_0B'), \tag{3.2}$$

$$\frac{\partial B'}{\partial t} + u' \frac{\partial B_0}{\partial x} = \left(\frac{\partial^2}{\partial x^2} + \frac{\partial^2}{\partial y^2} \right) B' - D_a(A'B_0 + A_0B'), \tag{3.3}$$

$$\frac{\partial C'}{\partial t} + u' \frac{\partial C_0}{\partial x} = \left(\frac{\partial^2}{\partial x^2} + \frac{\partial^2}{\partial y^2} \right) C' + D_a(A'B_0 + A_0B'), \tag{3.4}$$

$$\mu' = \mu_0(R_b B' + R_c C'). \tag{3.5}$$

Applying the curl to Darcy's equation and using the continuity equation gives

$$\mu_0 \left(\frac{\partial^2}{\partial x^2} + \frac{\partial^2}{\partial y^2} \right) u' + \frac{\partial \mu_0}{\partial x} \left(\frac{\partial u'}{\partial x} \right) = -\frac{\partial^2 \mu'}{\partial y^2}. \tag{3.6}$$

Using the expression for the viscosity disturbance (3.5), the right-hand side of (3.6) is further simplified to

$$\left(\frac{\partial^2}{\partial x^2} + \frac{\partial^2}{\partial y^2} \right) u' + \frac{1}{\mu_0} \frac{\partial \mu_0}{\partial x} \frac{\partial u'}{\partial x} = -R_b \frac{\partial^2 B'}{\partial y^2} - R_c \frac{\partial^2 C'}{\partial y^2}. \tag{3.7}$$

3.2. *Quasi-steady-state approximation*

The coefficients of these linearized equations are a function of space and time as the base state is spatially and temporally varying. To solve the problem, we therefore use a quasi-steady-state approximation (QSSA) whereby the base-state solutions are 'frozen' at a time t_0 (Tan & Homsy 1986). The stability of this frozen profile is then determined by expanding the disturbances in terms of Fourier components as

$$(u', A', B', C') = (\phi, \psi_A, \psi_B, \psi_C) e^{iky + \sigma(t_0)t}, \tag{3.8}$$

where ψ_A, ψ_B and ψ_C are only functions of x while $\sigma(t_0)$ is the growth rate of a disturbance of wavenumber k. Inserting the above normal mode expansions into the linearized equations (3.2)–(3.4) and (3.7) and eliminating the amplitude of the product perturbation ψ_C using the relation $\psi_A + \psi_B + 2\psi_C = 0$ leads to:

$$\left[\frac{\mathrm{d}^2}{\mathrm{d}x^2} + \left(\left[R_b - \frac{R_c}{2} \right] \frac{\partial B_0}{\partial x} - \frac{R_c}{2} \frac{\partial A_0}{\partial x} \right) \frac{\mathrm{d}}{\mathrm{d}x} - k^2 \right] \phi = k^2 \left(\left[R_b - \frac{R_c}{2} \right] \psi_B - \frac{R_c}{2} \psi_A \right), \tag{3.9}$$

$$\left[\sigma(t_0) - \frac{\mathrm{d}^2}{\mathrm{d}x^2} + k^2 + D_a B_0 \right] \psi_A = -\frac{\partial A_0}{\partial x} \phi - D_a A_0 \psi_B, \tag{3.10}$$

$$\left[\sigma(t_0) - \frac{\mathrm{d}^2}{\mathrm{d}x^2} + k^2 + D_a A_0 \right] \psi_B = -\frac{\partial B_0}{\partial x} \phi - D_a B_0 \psi_A. \tag{3.11}$$

The above eigenvalue system of differential equations is next solved to determine the growth rates $\sigma(t_0)$ using two approaches. The first approach discussed in §4 is based on step profiles for the reactants base-state concentrations ($t_0 = 0$) and results in an algebraic equation for the growth rate. The second approach is presented in §5 and involves a numerical solution of the system (3.9)–(3.11).

4. Dispersion curves at $t_0 = 0$

4.1. *Analytical solution at $t_0 = 0$*

An analytical solution for the growth rate σ at $t_0 = 0$ will now be derived. The concentrations of the two reactants are represented using the Heaviside step function:

$$A_0 = H(-x) = \begin{cases} 1 & x < 0 \\ 0 & x > 0, \end{cases} \qquad B_0 = H(x) = \begin{cases} 0 & x < 0 \\ 1 & x > 0. \end{cases} \tag{4.1}$$

For $x < 0$, the linearized equations therefore are

$$\left[\frac{d^2}{dx^2} - k^2\right]\phi = k^2\left(\left[R_b - \frac{R_c}{2}\right]\psi_B - \frac{R_c}{2}\psi_A\right), \tag{4.2}$$

$$\left[\sigma - \frac{d^2}{dx^2} + k^2\right]\psi_A = -D_a\psi_B, \tag{4.3}$$

$$\left[\sigma - \frac{d^2}{dx^2} + k^2 + D_a\right]\psi_B = 0. \tag{4.4}$$

The solutions of the above equations are

$$\left.\begin{aligned}
\psi_B^- &= B^- e^{\gamma_0 x},\\
\psi_A^- &= A^- e^{\gamma_1 x} + B^- e^{\gamma_0 x},\\
\phi^- &= G^- e^{kx} - \frac{R_c k^2}{2(\gamma_1^2 - k^2)}A^- e^{\gamma_1 x} - \frac{(R_c - R_b)k^2}{\gamma_0^2 - k^2}B^- e^{\gamma_0 x},
\end{aligned}\right\} \tag{4.5}$$

where A^-, B^- and G^- are constant coefficients while γ_0 and γ_1 are defined as follows:

$$\gamma_0 = \sqrt{k^2 + \sigma + D_a}, \qquad \gamma_1 = \sqrt{k^2 + \sigma}. \tag{4.6}$$

On the other hand, for $x > 0$ the linearized equations are

$$\left[\frac{d^2}{dx^2} - k^2\right]\phi = k^2\left(\left[R_b - \frac{R_c}{2}\right]\psi_B - \frac{R_c}{2}\psi_A\right), \tag{4.7}$$

$$\left[\sigma - \frac{d^2}{dx^2} + k^2 + D_a\right]\psi_A = 0, \tag{4.8}$$

$$\left[\sigma - \frac{d^2}{dx^2} + k^2\right]\psi_B = -D_a\psi_A. \tag{4.9}$$

The corresponding solutions are

$$\left.\begin{aligned}
\psi_A^+ &= A^+ e^{-\gamma_0 x},\\
\psi_B^+ &= B^+ e^{-\gamma_1 x} + A^+ e^{-\gamma_0 x},\\
\phi^+ &= G^+ e^{-kx} - \frac{(R_c - R_b)k^2}{\gamma_0^2 - k^2}A^+ e^{-\gamma_0 x} + \frac{(R_b - \frac{R_c}{2})k^2}{\gamma_1^2 - k^2}B^+ e^{-\gamma_1 x},
\end{aligned}\right\} \tag{4.10}$$

where A^+, B^+ and G^+ are constant coefficients. The arbitrary constants in (4.5) and (4.10) are determined by applying the following continuity conditions at $x = 0$:

$$\left.\begin{aligned}
&\left[\mu_0\frac{d\phi}{dx}\right]_{0^-}^{0^+} = 0, \quad [\phi]_{0^-}^{0^+} = 0,\\
&\left[\frac{d\psi_A}{dx}\right]_{0^-}^{0^+} = -\phi(0), \quad [\psi_A]_{0^-}^{0^+} = 0,\\
&\left[\frac{d\psi_B}{dx}\right]_{0^-}^{0^+} = \phi(0), \quad [\psi_B]_{0^-}^{0^+} = 0.
\end{aligned}\right\} \tag{4.11}$$

The above conditions are obtained by integrating (3.9)–(3.11) across $x = 0$. Imposing these conditions results in a homogeneous system of six algebraic equations for the unknowns. For non-trivial solutions, the determinant of the coefficient matrix is required to be zero, which results in the following nonlinear equation relating implicitly the growth rate σ to the disturbance wavenumber k:

$$-2\gamma_0 \left[(e^{R_b} + 1) \left\{ \frac{(R_c - R_b)k^2}{\gamma_0^2 - k^2}(\gamma_0 - k) + \frac{(2R_b - R_c)k^2}{\gamma_1^2 - k^2}(\gamma_1 - k) - 2k\gamma_1 \right\} \right.$$

$$\left. + 2\frac{(R_c - R_b)k^2}{\gamma_1^2 - k^2}(\gamma_1 - k) - 2\frac{(R_c - R_b)k^2}{\gamma_0^2 - k^2}(\gamma_0 - k) \right] = 0. \quad (4.12)$$

The above equation may be further simplified to

$$(e^{R_b} + 1)(\gamma_0 + k)[R_b k - 2\gamma_1(k + \gamma_1)] + k(e^{R_b} - 1)(R_c - R_b)(\gamma_1 - \gamma_0) = 0. \quad (4.13)$$

The stability of the problem depends on the value of σ, which in general may be complex. The system is stable if $\mathrm{Re}(\sigma)$ is negative for all values of k and unstable if $\mathrm{Re}(\sigma)$ is positive for some k. Plotting the real part of the growth rate $\mathrm{Re}(\sigma)$ against the wavenumber k yields dispersion curves that we will now seek to obtain for various values of the flow parameters. The various types of dispersion curves will be classified using the definitions given by Cross & Hohenberg (1993). Type I dispersion curves cross the line $\mathrm{Re}(\sigma) = 0$ at the three wavenumbers $k = 0$, k_1 and k_2 such that growth rates with positive real parts occur for $0 < k_1 < k < k_2$. Such dispersion curves lead to fingers maintaining a finite wavenumber in time (Bánsági *et al.* 2003) and long-wave instabilities are absent. Type II dispersion curves cross the line $\mathrm{Re}(\sigma) = 0$ at the two wavenumbers $k = 0$ and k_c such that growth rates with positive real parts occur for $0 < k < k_c$. Such dispersion curves can include long-wave instabilities in which fingers appear with a zero wavenumber and are characterized in the nonlinear regime by a general coarsening trend in time. As (4.13) satisfies $\sigma = k = 0$, type III dispersion curves (for which $\sigma \neq 0$ at $k = 0$) are not possible.

First, note that in the limit of an infinitely slow reaction, i.e. $D_a \to 0$, one has $\gamma_0 \to \gamma_1$ and (4.13) reduces to

$$\sigma = \frac{k}{2}(R_b - k - \sqrt{k(k + 2R_b)}), \quad (4.14)$$

which is the classical dispersion equation for miscible viscous fingering in non-reactive fluids obtained by Tan & Homsy (1986). Equation (4.14) corresponds to a type II dispersion curve because $\sigma > 0$ for $0 < k < R_b/4$. The maximum growth rate $\sigma_m R_b^2$ occurs at the most unstable wavenumber $k_m R_b$ where $k_m = (\sqrt{5} - 2)/2$ and $\sigma_m = (5\sqrt{5} - 11)/8$. In the absence of reactions, the system is thus unstable whenever $R_b > 0$.

Equation (4.14) is also obtained from (4.13) when $R_b = R_c$, which is expected because, as already explained earlier, if the reaction is converting B to C with $\mu_B = \mu_C$ then the resulting system is equivalent to the non-reactive case. Note that although species A is being consumed, the change in its concentration does not affect the flow viscosity that is normalized by μ_A.

Let us now seek to find the various zones of instabilities at $t_0 = 0$ in the (R_b, R_c) parameter plane.

4.2. *Long-wave instabilities*

A long-wave instability is sought by letting k and σ be small in (4.13). It was found that, in order to balance the equation, σ and k must be of the same order. Hence, they are expressed as $\sigma = \epsilon W$ and $k = \epsilon K$, where ϵ is small and positive. Expanding (4.13) in ϵ yields

$$2\epsilon W \sqrt{D_a}(e^{R_b} + 1) = \epsilon K \sqrt{D_a}(R_c + (2R_b - R_c)e^{R_b}) + O(\epsilon^{3/2})$$
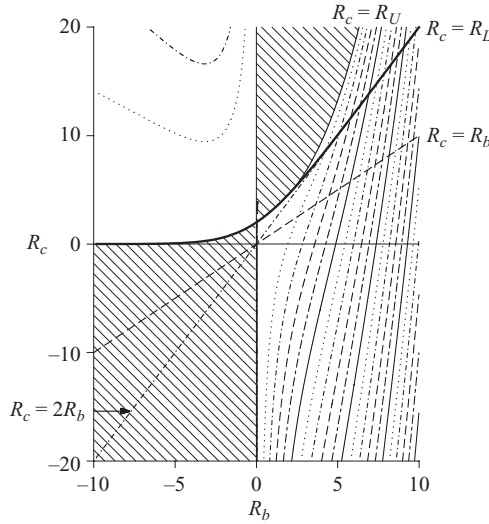
FIGURE 4. Contours of the maximum growth rate in the (R_b, R_c) plane for $D_a = 1$ at $t_0 = 0$. The shaded regions are stable. The contours of the maximum growth rate are illustrated at equal intervals of 0.15. For $R_b > 0$, the system is unstable for $R_c < R_U$, while instability occurs if $R_c > R_L$ for $R_b < 0$.

for $D_a > 0$. Therefore

$$\frac{W}{K} = \frac{R_c + (2R_b - R_c)e^{R_b}}{2(e^{R_b} + 1)} + O(\epsilon^{1/2}).$$

The condition on the parameters R_b and R_c at which the onset of an instability occurs is called the neutral stability curve. Because W is real, the neutral stability curve is obtained by substituting $W = 0$ in the above equation, which shows that a long-wave instability occurs at $R_c = R_L$, where

$$R_L = \frac{2R_b}{1 - e^{-R_b}}. \tag{4.15}$$

Note that $R_L > 0$ for all values of R_b. For $W \geqslant 0$ one requires that $R_c + (2R_b - R_c)e^{R_b} \geqslant 0$, i.e. $R_c(1 - e^{-R_b}) \leqslant 2R_b$. Hence, the system is unstable for $R_c < R_L$ if $R_b > 0$ and for $R_c > R_L$ if $R_b < 0$ (see figure 4). It should be stressed that the curve $R_c = R_L$ is not always the neutral stability curve because short-wave instabilities or complex growth rates exist for $R_L < R_C < R_U$ (see the Appendix), where R_U is determined numerically but detailing these trends is beyond the scope of this work. The zones of instabilities are summarized by plotting the contours of maximum growth rate in the (R_b, R_c) plane for $D_a = 1$ at $t_0 = 0$ in figure 4.

4.3. *Parametric study*

In this section, the effects on the instability of the Damköhler number D_a and the parameter R_c are examined. The role of these two parameters has already been the subject of earlier experimental studies. In particular, fast and slow chemical reactions corresponding to large and small D_a have been examined by Nagatsu *et al.* (2007) and Nagatsu *et al.* (2009), respectively. There are also experiments on cases where the chemistry either increases ($R_c > 0$) (Nagatsu *et al.* 2007; Podgorski *et al.* 2007) or decreases ($R_c < 0$) (Nagatsu *et al.* 2007) the viscosity.
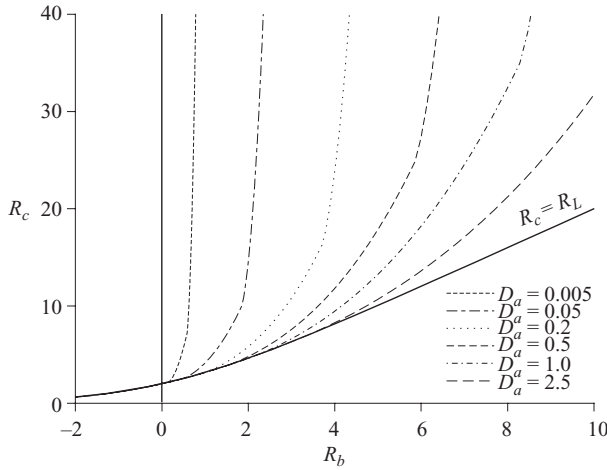
FIGURE 5. Neutral stability curves for various values of D_a at $t_0 = 0$. For $R_b > 0$, the system is unstable below the D_a-dependent curve.

4.3.1. *Effects of D_a*

Figure 5 shows the neutral stability curves for various values of D_a at $t_0 = 0$, with the curves $R_b = 0$ and $R_c = R_L$ shown by solid lines. For $R_b = 0$, the flow is stable regardless of the values of R_c or D_a at $t_0 = 0$. For an initially stable viscosity profile ($R_b < 0$), the flow is unstable if $R_c > R_L$. Note that the neutral curves for this case are independent of D_a. On the other hand, in the case of initially unstable viscosity profile ($R_b > 0$), the flow is unstable if $R_c < R_L$. For $R_U > R_c > R_L$, the flow is stable to long-wave disturbances but is unstable to short waves (type I curves). In the latter case, the neutral curves depend on D_a.

We now discuss the effect of the reaction rate. As $D_a \to 0$, the neutral stability curve approaches the line $R_b = 0$ which is logical, as one then recovers the non-reactive situation for which the whole half-plane where $R_b > 0$ is unstable.

Concerning the value of the most unstable mode, let us note that taking the limit $D_a \to \infty$, i.e. taking the limit of an infinitely fast reaction, reduces (4.13) to

$$\sigma = \frac{k}{2}(p - k - \sqrt{k(k + 2p)}), \tag{4.16}$$

where

$$p = R_b + \left(\frac{e^{R_b} - 1}{e^{R_b} + 1}\right)(R_b - R_c) = \left(\frac{e^{R_b} - 1}{e^{R_b} + 1}\right)(R_L - R_c). \tag{4.17}$$

The maximum growing wavenumber is $k_m p$ and the maximum growth rate is $\sigma_m p^2$. This shows again that the non-reactive case (4.14) is recovered in the special case where $R_c = R_b$, i.e. when $p = R_b$. The neutral stability curve is at $p = 0$, i.e. $R_c = R_L$. For the system to be unstable for $D_a \to \infty$, one requires that $p > 0$; therefore, it is necessary that $R_c < R_L$ if $R_b > 0$, and $R_c > R_L$ if $R_b < 0$. Furthermore, for large R_b, the line $R_c = R_L$ approaches the line $R_c = 2R_b$. Note that this line is precisely the one for which the viscosity profile switches from monotonic to non-monotonic in the long time limit.

Let us now determine whether the unstable reactive system is more or less unstable than its non-reactive equivalent. To do so, the effect of D_a on the stability of the system at $t_0 = 0$ is illustrated in figure 6.
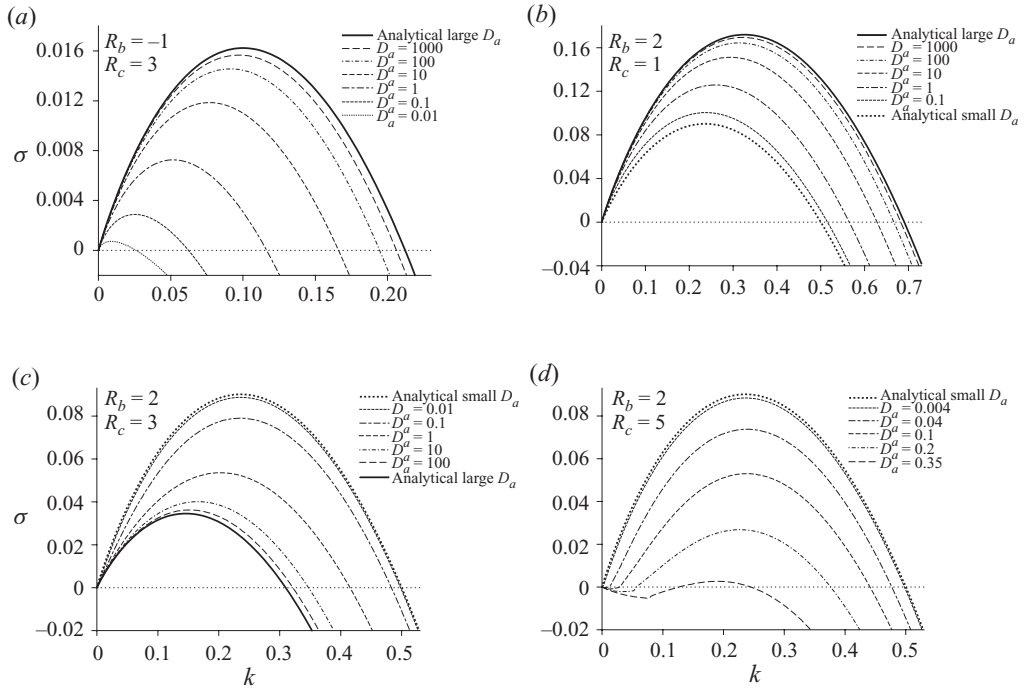
FIGURE 6. Dispersion curves at $t_0 = 0$ showing the influence of the Damköhler number D_a for (*a*) $R_b = -1$ and $R_c = 3$, (*b*) $R_b = 2$ and $R_c = 1$, (*c*) $R_b = 2$ and $R_c = 3$ and (*d*) $R_b = 2$ and $R_c = 5$.

If $R_b < 0$, the system is stable for the non-reactive case $D_a = 0$ while the most unstable situation is obtained for $D_a \to \infty$ when the dispersion curve approaches the analytical solution given by (4.16) as shown in figure 6(*a*). Decreasing D_a causes the system to become less unstable, i.e. both the maximum growth rate and the band of unstable modes decrease. Eventually, the system reaches the stable non-reactive situation of a more viscous fluid pushing a less viscous one when $D_a = 0$.

If $R_b > 0$, the initial front between the two reactants A and B is genuinely unstable. In this case, one notes that p in (4.17) can be equal to R_b only when $R_c = R_b$ and in this case, the system behaves like the non-reactive one. Out of this line, the influence of the reaction can have different trends. For $D_a \to \infty$, (4.17) reveals that in the region $R_b < R_c$, $p < R_b$ and so the chemical reaction has a stabilizing effect with both the maximum growing wavenumber and maximum growth rate being smaller than their corresponding non-reactive counterparts for the same value of R_b. On the contrary, in the region $R_c < R_b$, $p > R_b$ and therefore the chemical reaction has now a destabilizing effect. So, in short, if the reaction is dominant in the dynamics ($D_a \to \infty$) and the system is genuinely unstable ($R_b > 0$) because the displacing solution of A is less viscous than the solution of B, the reaction tends to further destabilize the system if $R_c < R_b$ and to stabilize it otherwise. Let us illustrate this for specific points in the $R_b > 0$ part of the (R_b, R_c) plane.

Figure 6(*b*) illustrates the influence of D_a in the case $R_c < R_b$. As shown on the viscosity profiles of figure 2(*a*), this corresponds to situations with a larger viscosity gradient at the leading zone. Increasing D_a causes the system to become more unstable as more product C is produced per unit of time. As D_a tends to zero or infinity, the

dispersion curve approaches the analytical solutions (4.14) of the non-reactive system and (4.16) for $D_a \rightarrow \infty$, respectively.

Opposite effects are observed when $R_c > R_b$ in which case an increase of D_a leads to a less unstable system. Figure 6(c) illustrates these trends when $R_L > R_c > R_b$. The limiting case $D_a \rightarrow \infty$ corresponds to the least unstable flow while the non-reactive one results in the most unstable flow. For $R_U > R_c > R_L > R_b$, chemical reaction still attenuates the instability but, moreover, it switches the dispersion curve from type II to type I. This is expected because as discussed in § 4.2, the flow is stable to long-wave disturbances when $R_c > R_L$ for $R_b > 0$. Therefore, there is now a critical value of D_a above which the system becomes stable. For the special values considered in figure 6(d), $R_b = 2$ and $R_c = 5$, the critical D_a is 0.375.

Let us insist that the trends for enhancement of the instability when $R_b < 0$ or when $R_b > 0$ and $R_b > R_c$ and its attenuation when $R_c > R_b > 0$ were found consistently for a wide range of mobility ratios and Damköhler numbers. This is also true for the change of dispersive curves from type II to type I with increasing Damköhler number when $R_U > R_c > R_L > R_b > 0$.

Having identified the effects of D_a on the initial stability of the system, let us now examine the effects of R_c.

4.3.2. *Effects of R_c*

The effects of R_c are illustrated in figure 7 for $D_a = 1$. If $R_b < 0$, as R_c is decreased the flow becomes less unstable, with a full stabilization once $R_c < R_L$. These trends are illustrated in figure 7(a) for $R_b = -1$ with a corresponding $R_L \approx 1.164$.

Instability characteristics when $R_b > 0$ are depicted in figure 7(b,c). Here the flow becomes less unstable with increasing R_c. In figure 7(b), the flow is fully stabilized once R_c reaches R_L, which in this particular case is $R_L \approx 3.164$. Further increase of R_c maintains a stable system. On the other hand, when the flow is still unstable when R_c reaches R_L, then, as predicted from the long-wave instability analysis, the flow ceases to be unstable at short wavelengths and type I dispersion curves are obtained. Ultimately, for large enough R_c, the flow is stabilized. These trends are illustrated in figure 7(c) where $R_b = 5$ and a corresponding $R_L \approx 10.068$.

In summary, an increase of R_c has a destabilizing effect if $R_c > R_L$ in the case where the non-reactive system is genuinely stable ($R_b < 0$). On the other hand, if the system is already viscously unstable even without reaction ($R_b > 0$), the production of an increasingly more viscous product, i.e. an increase of R_c has a stabilizing effect. In this latter scenario, type I dispersion curves are obtained if the flow is still unstable when R_c reaches R_L, while otherwise only type II dispersion curves should be expected.

4.4. *Summary*

The results of the stability analysis at $t_0 = 0$ can be summarized in terms of the three major parameters: R_b, R_c and D_a. When the initial non-reactive system is stable ($R_b < 0$), then faster chemical reactions (larger D_a) work towards increasing the instability. Furthermore, an increase in the viscosity of the chemical product C (larger R_c) tends to enhance the flow instability as long as $R_c > R_L$. For $R_c < R_L$, the flow is totally stable. If on the other hand the initial non-reactive system is genuinely unstable ($R_b > 0$) then faster chemical reactions tend to increase the flow instability if $R_c < R_b$ and to decrease it otherwise. In the latter case, the flow can be fully stabilized if $R_c > R_L$ while it remains unstable for all values of D_a if $R_c < R_L$. Finally, the more viscous the chemical product, i.e. the larger R_c, the less unstable is the flow. All these trends are summarized in a convenient way using a contour plot of the maximum
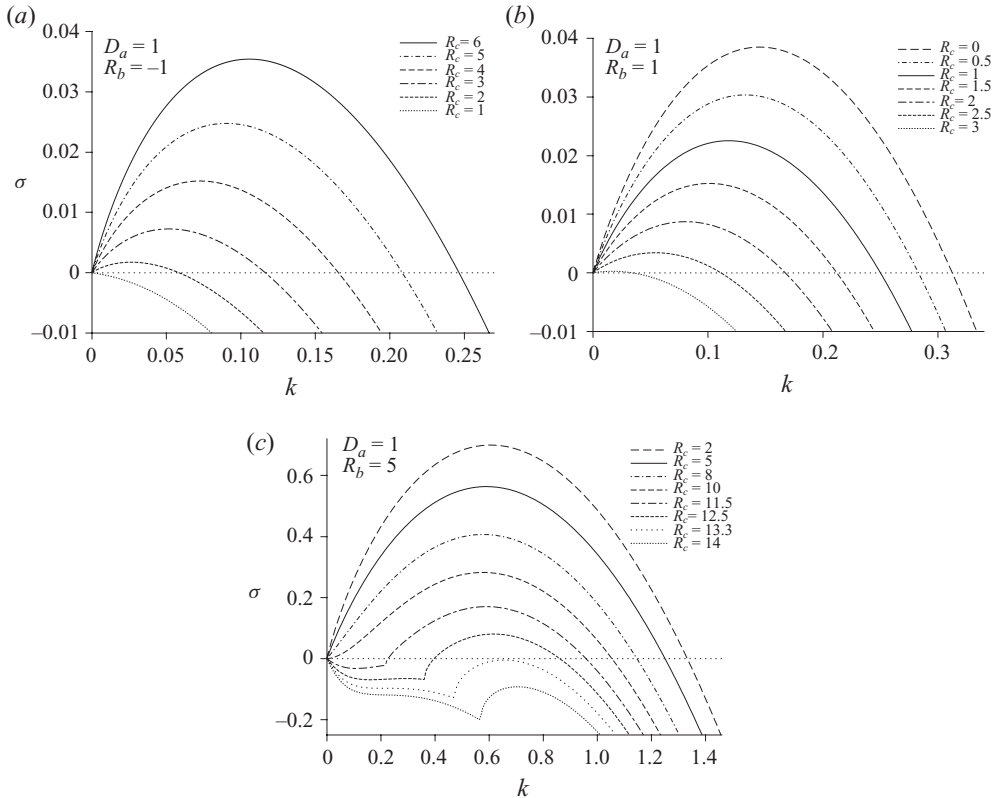
FIGURE 7. Influence of changes in R_c on dispersion curves at $t_0 = 0$ with $D_a = 1$ for (a) $R_b = -1$, (b) $R_b = 1$ and (c) $R_b = 5$. In (b, c) the full curve is the non-reactive equivalent obtained when $R_c = R_b$.

growth rate in the (R_b, R_c) plane for $D_a = 1$. Figure 4 represents the trends with the contours taking the value zero on the neutral stability curve (solid lines) and increasing away from it.

We should finally comment that formally, the QSSA is strictly not valid at $t_0 = 0$ as the base-state solution varies quickly at $t_0 = 0$. Moreover, it is difficult to get a physical interpretation of the results at $t_0 = 0$ because this corresponds to a situation where no diffusion has taken place yet. However, the results of the stability analysis at $t_0 = 0$ provide a useful starting point to understand where the instabilities are most likely to occur and develop in the parameter space. As shown in the next section, the stability characteristics at $t_0 = 0$ carry indeed the essence of the relative properties at later time. As time increases, the use of the QSSA is more justified as the rate of change of the base-state solution decreases. The next section discusses results of the LSA for such times greater than zero.

5. Stability at later times

In the preceding section, the stability of the reactive system at $t_0 = 0$ was analysed. At later times, the stability properties can be modified as the chemical reaction changes the base state of the problem in time. As time goes by, more chemical product is generated while the reactants are consumed, which modifies the weight of each species

in the viscosity profile across the reaction zone. To gain insight into the development of the instability in time, the eigenvalue problem described by (3.9)–(3.11) is solved numerically using a finite difference method and the RD base state at any given time is obtained by solving (2.16)–(2.18). A non-uniform grid that is finest around the interface where the concentration gradients are large is adopted. The computational domain is chosen wide enough to capture all eigenfunctions and to satisfy the decaying conditions at the boundaries. By discretizing the set of ordinary differential equations, the system results in a generalized algebraic eigenvalue problem. The general real matrix is converted into an upper Hessenberg form in order to obtain the eigenvalues and eigenfunctions. From the set of obtained discrete eigenvalues only the largest one is reported. The accuracy and convergence of the numerical results were ascertained by varying the domain length and the spatial step size. The code was validated by comparing with the results of Tan & Homsy (1986) for non-reactive flows ($D_a = 0$). Furthermore, excellent agreement between the predictions of the numerical code for small t_0 and the analytical results based on the step profile approximation were obtained. In the next sub-sections the cases where the initial reactant front is either stable ($R_b = 0$ or $R_b < 0$) or unstable ($R_b > 0$) will be examined.

5.1. *Equal reactant viscosities* ($R_b = 0$)

When the two reactants A and B have the same viscosity, $\mu_A = \mu_B$, then the initial non-reactive system is stable. However, once a reaction takes place ($D_a > 0$), a non-monotonic viscosity profile will develop if the viscosity of the chemical product C is different from that of the reactants, i.e. if $R_c \neq 0$. This viscosity profile will exhibit a maximum if $R_c > 0$ and a minimum if $R_c < 0$, and the resulting flow is expected to be unstable. However, a question may arise as to whether the system will be unstable right away at $t_0 = 0$ or whether there is a critical onset time for the instability to take place. One may also wonder whether chemical reactions that generate a product more viscous than the reactants ($R_c > 0$) will lead to different dynamics than those where the product is less viscous than the reactants ($R_c < 0$).

First, one should recall that for $t_0 = 0$ the flow is always stable when $R_b = 0$ (figure 4). However, it is expected that beyond a certain critical time, an instability will set in if $R_c \neq 0$. Figure 8(a) depicts the temporal evolution of the maximum growth rate for two selected values of fixed $|R_c|$ with $R_b = 0$ and $D_a = 1$. It is clear that indeed the system is not right away unstable as there is a threshold time for the instability to set in. This onset time which is dependent on the rate of production of C, logically increases when $|R_c|$ decreases, i.e. when the amplitude of the instability-driving force decreases. This result should be compared with that of Gérard & De Wit (2009), who used nonlinear simulations to analyse the case $R_b = 0$. Figure 2 of Gérard & De Wit (2009) showing the results of the simulations for $R_b = 0$, $R_c = 3$ and $D_a = 1$ indicates that the instability starts to develop around $t_0 = 100$. This time is of the same order of magnitude as the time when σ_{max} reaches its maximum value in time (figure 8a). Clearly, the results of the present LSA based on the QSSA are in good agreement with the nonlinear simulations.

Figure 8(a) also indicates that for a given $|R_c|$, the instability starts earlier when $R_c < 0$ than when $R_c > 0$. This shows that, for equal amplitude of the extremum, the system is more unstable when the reaction builds up a minimum rather than a maximum in the viscosity profile. This is related to the fact that fingers develop more easily along the flow on the leading zone than against the flow on the trailing zone (Mishra, Martin & De Wit 2008). However, at large times, the maximum growth rate becomes independent of the sign of R_c. It is suspected that this occurs when
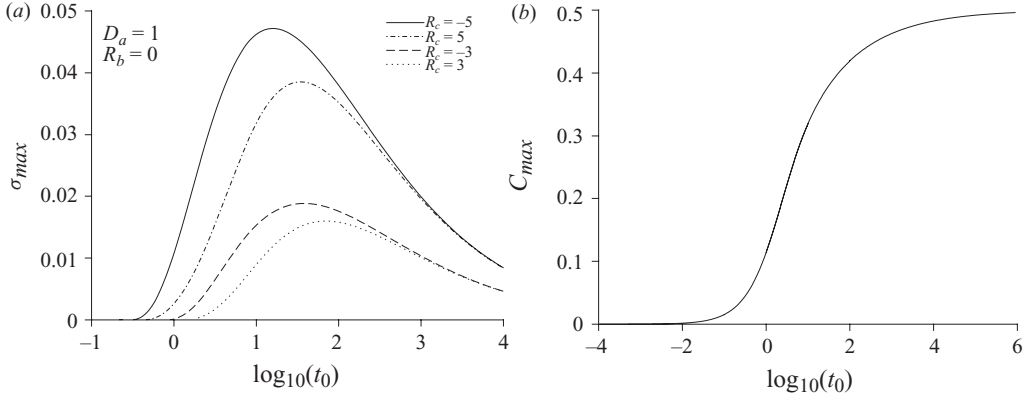
FIGURE 8. (a) Maximum instantaneous growth rate against $\log_{10}(t_0)$ when $R_b = 0$ and $D_a = 1$. (b) Maximum value of C for the RD problem against $\log_{10}(t_0)$ when $D_a = 1$.

the production of C levels off (see figure 8b). Finally, note that all curves of the maximum growth rate σ_{max} show a maximum at some intermediate time, indicating that the most unstable flow should be expected when enough chemical product has been generated but before the reaction levels off. After this time, the extremum in viscosity, i.e. the driving force of the instability, is then saturating, while diffusion smoothes the viscosity gradients out and hence stabilizes the system again.

5.2. *Stable initial reactant front* ($R_b < 0$)

In the left part of the (R_b, R_c) plane where the non-reactive situation is genuinely stable, the flow is expected to be unstable for $R_c > 0$ or $R_c < 2R_b < 0$ (figure 3). For $t_0 = 0$, it was found that the system is unstable only if $R_c > R_L > 0$. As shown below the situation is different for $t_0 > 0$.

5.2.1. $R_c > 0$

As time goes by, quite rapidly the whole upper left region, i.e. quadrant IV of figure 3, ultimately becomes unstable. This is expected as the non-monotonic viscosity profile features there a maximum with an unstable trailing zone and a stable leading one. A systematic parametric study has been conducted for negative R_b and different values of D_a and R_c in region IV. Typical trends for increasing instability with increasing Damköhler number at fixed R_c are illustrated in figure 9(a). This is associated with an increase in the rate of chemical production and thus with a larger maximum viscosity for a given fixed time. However, it should be noted that a further increase in D_a can in fact lead to a reduction of the instability.

For a fixed D_a but now increasing positive R_c, the maximum value of the viscosity profile increases; see figure 9(b). It should be stressed that these trends in $R_b < 0$ are similar to those reported in the nonlinear simulations by Gérard & De Wit (2009) in the special case $R_b = 0$ but $R_c > 0$, where indeed destabilization with increased D_a at fixed R_c or with increased R_c at fixed D_a is observed.

The temporal evolution of the maximum growth rate σ_{max} for $D_a = 1$, $R_b = -1$ and two positive values of R_c, namely $R_c = 2$ and $R_c = 4$, is depicted in figure 10(a). Clearly, the larger R_c the larger is the instantaneous maximum growth rate. Furthermore, σ_{max} reaches a maximum at an intermediate time before decaying fast at large times. It is worth noting that the maximum growth rate also exhibits a local minimum that is particularly noticeable in the case $R_c = 4$. Finally, note that these results are consistent
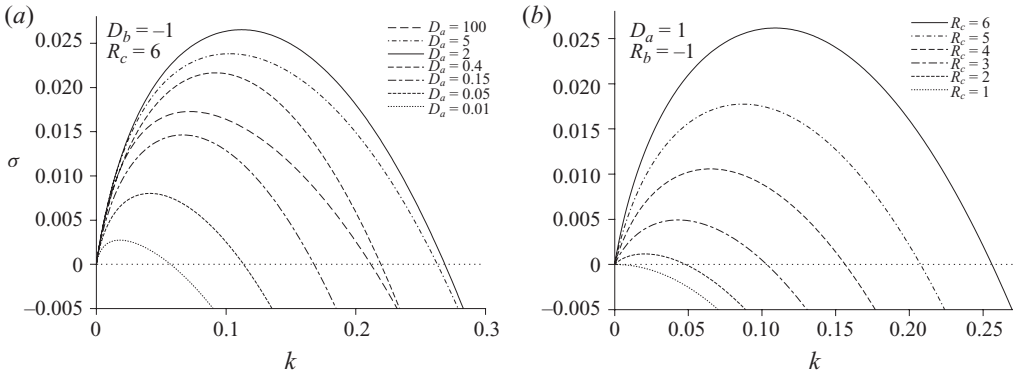
FIGURE 9. Instability characteristics at $t_0 = 1$ for zone IV: Trailing zone unstable, leading region stable. $R_b = -1$, (a) $R_c = 6$ and variable D_a, (b) $D_a = 1$ and variable R_c.
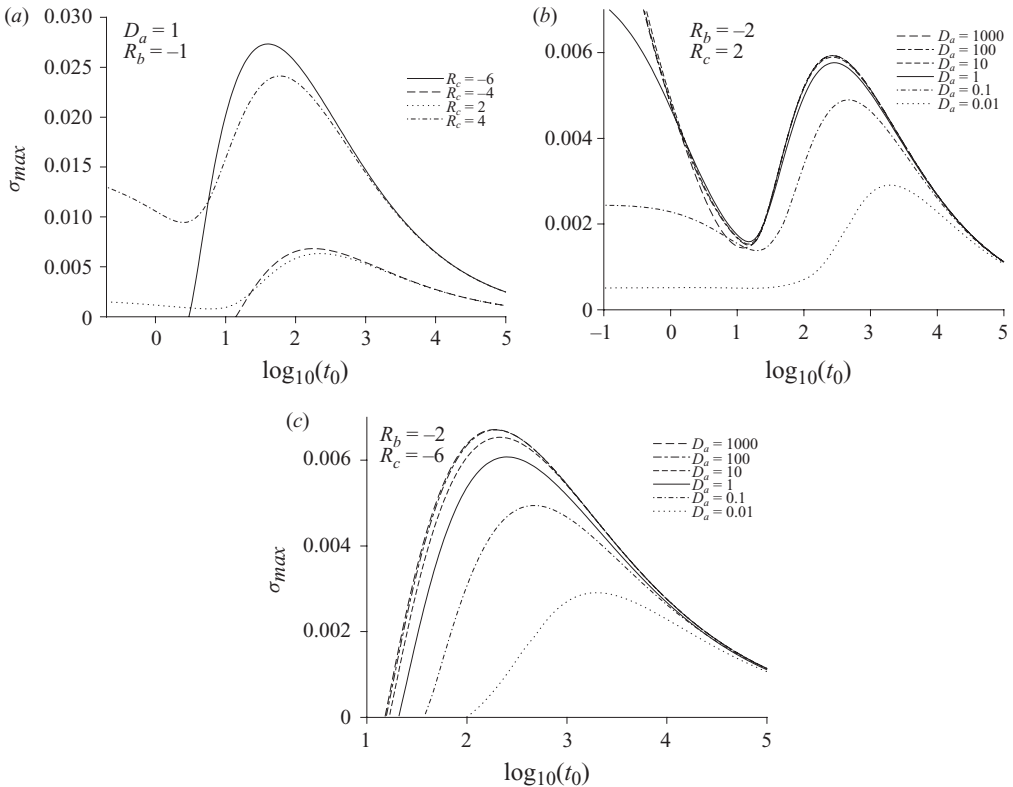

FIGURE 10. Maximum instantaneous growth rate against $\log_{10}(t_0)$ for (a) $D_a = 1$, $R_b = -1$ and various values of R_c, (b) $R_b = -2$, $R_c = 2$ and various values of D_a and (c) $R_b = -2$, $R_c = -6$ and various values of D_a.

with the numerical simulation of Hejazi & Azaiez (2010) where it was found that the instability develops at $t \approx 250$ for $R_b = -1$ and $R_c = 3$.

Figure 10(b) depicts the variations of the maximum growth rates with time at $R_b = -2$ and $R_c = 2$ and different values of D_a. For sufficiently large times, the maximum growth rates increase with increasing D_a. However, in early times an

increase of D_a may reduce the instability and an overall non-monotonic trend is observed. The curves display a local minimum and local maximum, with the former fading away for very small Damköhler numbers. Furthermore, as a result of a slower rate of chemical reaction, the smaller the Damköhler number the later in time the maximum is observed. At very large times all curves collapse and D_a does not have any effect on the instability.

5.2.2. $R_c < 2R_b < 0$

Let us now analyse the situation where $R_c < 2R_b$ when $R_b < 0$ for which the reaction builds up in time a non-monotonic viscosity profile with a minimum such that the trailing zone is stable while the leading region is unstable. It was found that in general, an increase in D_a or $|R_c|$ enhances the instability, and that in particular the flow can be unstable for negative R_c. This latter result is to be contrasted with what was obtained for $t_0 = 0$ where it was found that the flow is stable if $R_c < R_L$, which, recalling that R_L is always positive, implies that the flow is, in that case, necessarily stable when $R_c < 0$.

The variations of the instantaneous maximum growth rate with time are shown in Figure 10. Variations for fixed $D_a = 1$, $R_b = -1$ and two negative values of $R_c < 2R_b$, namely $R_c = -4$ and $R_c = -6$ are illustrated in figure 10(a) while the effects of D_a for fixed $R_b = -2$ and $R_c = -6$, are depicted in figure 10(c). Clearly, a threshold time is needed before the flow becomes unstable, and like other previously discussed cases, σ_{max} reaches a maximum at some intermediate time before decaying rapidly later. The required threshold time decreases with increasing D_a. In this case, a larger Damköhler number results systematically in a more unstable flow and, for large times, all curves decay to the same value such that the maximum growth rates become independent of D_a. Note also that for the same value of $|R_c - R_b|$, which is equal to 5 for $R_c = 4$ and $R_c = -6$ and equal to 3 for $R_c = 2$ and $R_c = -4$, the long time σ_{max} is the same. Furthermore, for a fixed $|R_c - R_b|$, the maximum growth rate is obtained when the instability is located at the leading zone ($R_c \leqslant 0$) where fingers develop along the flow rather than at the trailing one ($R_c > 0$) where the fingers have to move against the flow at the back and against a stable barrier at their tip.

5.3. Unstable initial reactant front ($R_b > 0$)

In the right part of the (R_b, R_c) plane where the non-reactive situation is in itself already unstable, increasing time quickly destabilizes the whole $R_b > 0$ half-plane. The results of the numerical solution for small $t_0 > 0$ when $R_b > 0$ are qualitatively similar to those obtained for the step-function approximation at $t_0 = 0$. In particular, the chemical reaction enhances the instability when the leading zone is more unstable than the trailing one ($R_b > R_c$) and attenuates it in the opposite case. No effects are observed when both zones are equally unstable ($R_c = R_b$). Note that even though the trends are qualitatively similar, the stabilizing or destabilizing effects due to the chemical reaction are stronger in the case of a step profile ($t_0 = 0$) than at later times $t_0 > 0$.

Figure 11(a) depicts the variations of σ_{max} with time for $D_a = 1$, $R_b = 3$ and various values of R_c. For flows with $R_c > R_b$, namely the curves corresponding to $R_c = 6$ and $R_c = 9$, similar trends to what has been observed earlier are also seen here, i.e. there is an intermediate-time maximum of σ_{max} before a decay at late times. The effects of D_a when $R_c > R_b$ are shown in figure 11(b). Similar to the case observed in figure 10(b), the effect of D_a depends on time, i.e. for early times the instability is reduced with increasing D_a, while it is increased at late times. In
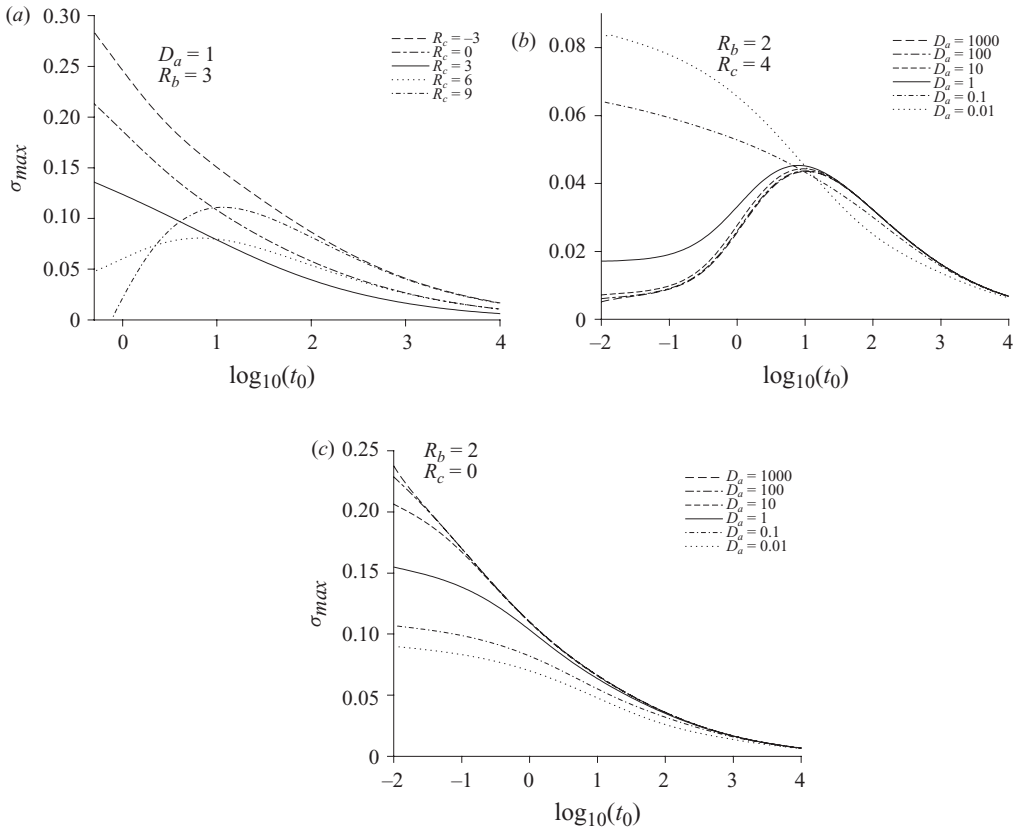
FIGURE 11. Maximum instantaneous growth rate against $\log_{10}(t_0)$ for (*a*) $D_a = 1$, $R_b = 3$ and various values of R_c, (*b*) $R_b = 2$, $R_c = 4$ and various values of D_a and (*c*) $R_b = 2$, $R_c = 0$ and various values of D_a.

the case $R_c < R_b$ namely the curves corresponding to $R_c = -3$, $R_c = 0$ and $R_c = 3$, the curves are monotonically decreasing, hinting that the maximum growth rate is reached at $t_0 = 0$. The effect of D_a for the case $R_c < R_b$ is shown in figure 11(*c*). Here, there is a systematic trend for increase of instability with increasing D_a.

   Note that the times at which the largest σ_{max} is reached are consistent with the times for the onset of instability in the nonlinear simulations of Hejazi & Azaiez (2010). Comparing the absolute maximum growth rate over time for fixed R_b and respectively the same $|R_b - R_c|$ shows that the non-monotonic profile is again more unstable when it exhibits a minimum, i.e. when the instability is located at the leading zone ($R_c \leqslant 0$) rather than at the trailing zone. Finally, note that the difference between these symmetric situations of constant $|R_b - R_c|$ vanishes at long times.

5.4. *Change of the instability in time*

The classical non-reactive VF is known to weaken in time when diffusion smoothes out unstable viscosity gradients (Tan & Homsy 1986; De Wit *et al.* 2005). Chemical reactions are obviously changing this picture as readily seen in figure 8 for $R_b = 0$. In this case, the system is stable at $t_0 = 0$ and positive growth rates are obtained only after a given onset time needed for the extremum in viscosity to build up. At later times, when the increase in the maximum concentration of the product C starts to level off (see figure 8*b*), σ_{max} starts to decrease. This can be attributed to a saturation of the
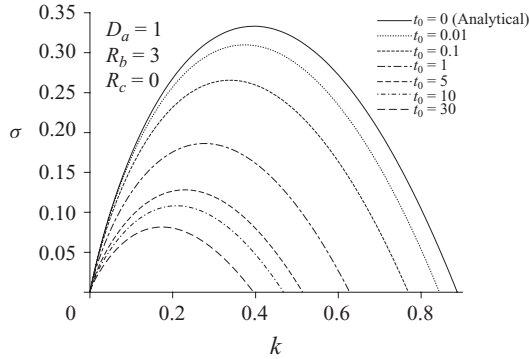
FIGURE 12. The QSSA growth constant versus wavenumber for different values of t_0, $R_b = 3$, $R_c = 0$ and $D_a = 1$.
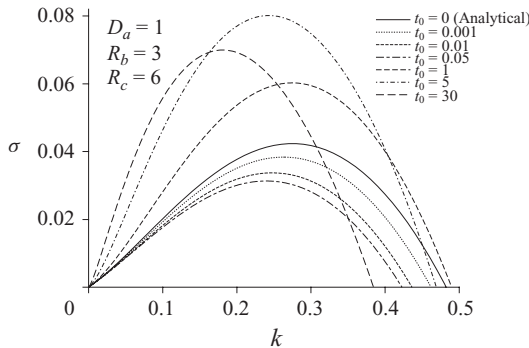

FIGURE 13. The QSSA growth constant versus wavenumber for different values of t_0, $R_b = 3$, $R_c = 6$, and $D_a = 1$.

destabilizing effects due to chemistry combined with the stabilizing effects of diffusion, which tends to smooth out the viscosity gradients between the different species.

A similar trend is observed for $R_b > 0$ where the situation furthermore depends on whether the system is unstable at $t_0 = 0$ or not. Figure 12 shows dispersion curves for different times starting from $t_0 = 0$ in the case $R_b = 3$, $R_c = 0$, i.e. when the trailing zone is neutrally stable and the leading one unstable. The trends observed for a reduction of the instability with increasing time are similar to what is already known in the case of non-reactive flows with monotonic viscosity profiles.

Figure 13 depicts the effect of diffusion in the opposite case where $R_b = 3$, $R_c = 6$, i.e. the trailing zone is unstable while the leading zone is neutrally stable. In this case, a non-monotonic temporal behaviour of the dispersion curves is observed. Up to a certain critical time $t_c \simeq 0.05$, an increase in time leads to a 'less' unstable flow, but at later times up to around $t_0 \simeq 5$ the growth rate increases. For larger times, the maximum growth rate and the spectrum of unstable wavenumbers are reduced with increasing time.

This non-monotonic variation of the instability characteristics with time can be attributed to the close interplay between chemistry and hydrodynamics. At early times, an increase of t_0 results in a reduction in the stabilization because of the stabilizing effect of the chemical reaction at small times. However, a little later there is more chemical product and therefore larger viscosity gradients and a stronger

instability. Recall that, unlike the previous case ($R_b = 3$, $R_c = 0$), here the instability grows in the trailing zone and develops opposite to the flow. For large enough D_a, this is able to mitigate the effects of diffusion. However, at still later times t_0, the chemical production saturates and diffusive effects become dominant. This interpretation is supported by the results for slow reactions (small D_a), where monotonic changes in time of the instability characteristics similar to those in figure 12 were obtained. This temporal difference in stability was well illustrated in figure 11(a).

Non-monotonic changes in the instability characteristics with time have also been found in the case $R_b < 0$, and as shown in figure 10(a), the situation can even be more complicated. At asymptotic long times, symmetric values of R_c around the line $|R_b - R_c|$ give the same growth rate but the situation is more unstable at intermediate times. There, systems where the instability is located on the leading zone are more unstable than their equivalent of the trailing region. The situation however is also different at time $t_0 = 0$, where the results summarized in §4 are recovered.

5.5. *Summary*

Trends of the flow instability and its change with time have been summarized by plotting stability zones and contours of the maximum growth rate in the (R_b, R_c) plane for $D_a = 1$. The results are shown in figure 14 for $t_0 = 0.5$, 1, 4 and 100 and have to be compared with those for $t_0 = 0$ presented in figure 4. Before analysing these contours, it is important to remember that these are instantaneous growth rates and the overall instability of the system actually depends cumulatively on the evolution of the growth rate in time.

If $R_b > 0$, the stable zone very quickly shrinks until ultimately the whole $R_b > 0$ half-plane becomes unstable. For $R_b < 0$, a comparison of figures 4 and 14 shows that while the whole quadrant VI ($R_c < 2R_b < 0$) of figure 3 is stable at $t_0 = 0$, an instability develops in the course of time, destabilizing first the system with small negative R_b and large negative R_c. This can be understood as, for small negative R_b, the stable initial reactant front can easily be destabilized by a strongly less viscous product giving a minimum of large amplitude in the viscosity profile and a destabilizing leading region. Ultimately, in the large time limit, only region V of figure 3 remains stable. This is expected as this is the only region where the viscosity profile remains monotonically decreasing.

For a given value of R_b, in the large time limit, the growth rates are found to be smallest on the line $R_c = R_b$ (see figure 14d). Furthermore, the instantaneous growth rates at large times are symmetrical about this line as the vertical distance to a contour of a given value is the same both above and below the line $R_c = R_b$. This implies that for large times the instantaneous growth rate eventually becomes independent of R_b when $R_c > R_b$. In figure 14(d) at $t_0 = 100$, the contours in the region $R_c > R_b$ have a negative gradient that decays to zero as R_c increases. Furthermore, in the region $R_c < R_b$, away from the line $R_c = R_b$ the contours have a positive gradient decaying to two as R_c decreases so that the contours are parallel to the line $R_c = 2R_b$.

Figure 14(d) also shows that at fixed $R_b > 0$ and large times, the maximum growth rate is increasing when R_c is decreased below zero. This corresponds to non-monotonic viscosity profiles with an increasing amplitude of the minimum (zone I in figure 3). On the other hand, in the upper right quarter where R_b and R_c are positive, we see that for $R_b \sim 10$, an increase of R_c first tends to stabilize the system as the viscosity gradient becomes steeper in the trailing zone and smoother in the leading zone. Once R_c is large enough, there is again a destabilization with increasing R_c, corresponding to an increase of the maximum in the non-monotonic profiles of region III in figure 3.
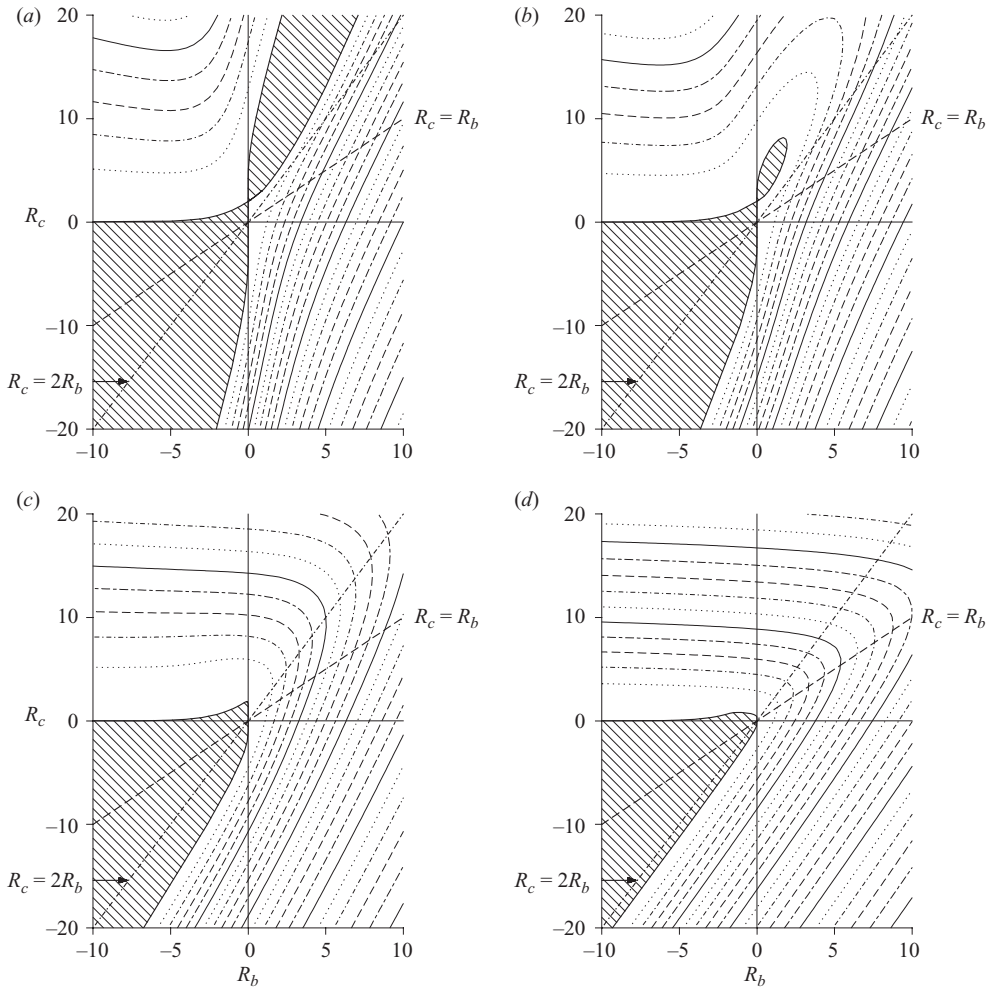
FIGURE 14. Contours of the maximum growth rate in the (R_b, R_c) plane for $D_a = 1$ at (a) $t_0 = 0.5$, (b) $t_0 = 1$, (c) $t_0 = 4$ and (d) $t_0 = 100$. The shaded regions are stable. The contours of the maximum growth rate are illustrated at equal intervals of (a) 0.05, (b) 0.04, (c) 0.03 and (d) 0.015.

The asymmetry between VF at the trailing versus leading zones discussed earlier is also well illustrated. In particular, this can be seen from an inspection of the maximum values of the growth rates at intermediate times (see figure 14b). For values of R_c equidistant from the line $R_c = R_b$, regions I ($R_c < 0$, $R_b > 0$) and VI ($R_c < 2R_b < 0$) of figure 3 for which the instability is located on the leading zone are respectively more unstable than regions III ($R_c > 2R_b > 0$) and IV ($R_c > 0$, $R_b < 0$) for which the instability is at the trailing zone.

6. Conclusion and discussion

Simple $A + B \rightarrow C$ chemical reactions have recently been shown both to influence experimentally and theoretically the properties of miscible viscous fingering when generating a product C having a viscosity different from that of the reactants A and

B. A detailed linear stability analysis of the problem has been performed to determine to what extent such a simple bimolecular reaction can modify the stability properties of a system where the reactant A is displacing a more or less viscous reactant B. This stability problem depends crucially on time as the base-state reaction–diffusion concentration profiles and hence the related viscosity profile change in time. Hence, we make the quasi-steady-state approximation to examine the stability of the base-state profiles at a time t_0. An analytical stability analysis is performed at time $t_0 = 0$ while a numerical approach is used at $t_0 > 0$.

Before discussing the results, let us summarize the main parameters and their significance. The rate of the chemical reaction is expressed by the Damköhler number D_a that accounts for the ratio of hydrodynamic and chemical characteristic times. The parameter R_b represents the ratio of the viscosity of the displaced reactant B to that of the displacing reactant A. Therefore, the initial front is stable when $R_b \leqslant 0$ and unstable otherwise. Furthermore, the ratio of the viscosity of the chemical product C to that of the displacing reactant A is represented by R_c. When $R_b < R_c$ ($R_b > R_c$), the leading reaction zone between the product C and the reactant B is less (respectively more) unstable than the trailing reaction zone between the reactant A and the product C. Finally, the leading reaction zone is stable when $R_c \geqslant 2R_b$ while the trailing one is stable when $R_c \leqslant 0$.

It was found that even if some zones (as summarized in figure 4) are stable at $t_0 = 0$, the chemical reaction quickly destabilizes almost all of the (R_b, R_c) parameter plane. As summarized in figure 14(d) for $t_0 = 100$, the only stable situation for long-time asymptotic reactive VF is when the chemical reaction maintains a monotonic decreasing viscosity profile (zone V in figure 3 for which $2R_b < R_c < 0$). All other situations for which the viscosity profile is either non-monotonic or monotonically increasing are destabilized. In these unstable situations, one then needs to check whether the chemical reaction leads to non-monotonic viscosity profiles or not.

For the non-monotonic cases, $R_c(R_c - 2R_b) > 0$, a maximum or a minimum in viscosity develops in time such that there will always be either a trailing or a leading region behind or ahead, respectively, of the reaction zone that features an unfavorable log-mobility ratio. In this case, an instability eventually always sets in and it increases with increasing $|R_c|$ at fixed R_b, i.e. for changes in the parameters that favour an increase of the amplitude of the extremum. The dependence on the Damköhler number D_a is more complicated. Indeed, it was found that for short times, faster chemical reactions reflected by a larger D_a always enhance the instability except in the case of an unstable initial system ($R_b > 0$) that gives rise to a trailing zone more unstable than the leading one ($R_c > R_b$). This picture does however get complicated as time passes by and faster reactions can in fact act towards reducing the instability.

If the viscosity profile is monotonically increasing, $R_c > 0$ and $(R_c - 2R_b) < 0$, the underlying non-reactive system is already unstable because a less viscous solution of A displaces a more viscous solution of B. However, the reaction modifies the stability properties because, unless $R_c = R_b$ which is the equivalent of the non-reactive case, the presence of the product C breaks the symmetry of the viscosity profile with regard to the reaction front position. It was found that the system is more unstable when the mobility ratio at the leading zone is larger than that at the trailing zone. Even in symmetric situations where $R_c = 0$ and $R_c = 2R_b$ for which the same unfavourable viscosity jump occurs at the leading and trailing regions, respectively, the situation is more unstable in the former case. This conclusion also holds in the case $R_b = 0$ where the flow is more unstable for viscosity profiles featuring a minimum ($R_c < 0$,

i.e. leading zone unstable and trailing zone stable) rather than a maximum ($R_c > 0$, i.e. leading zone stable and trailing zone unstable).

These differences in the trends that depend on whether the viscosity jump is larger on the trailing or leading zones and the asymmetric behaviour when both zones have the same viscosity jump may seem at first sight counterintuitive. However, as shown by Mishra *et al.* (2008) for non-reactive VF of finite slices, fingering is more intense for fingers extending along the flow than against it, i.e. for fingers developing on the leading zone of a non-monotonic viscosity profile rather than on the trailing zone. Therefore, here, for the same fixed viscosity jump, the instability is always more developed at the leading zone and attenuated at the trailing zone. In particular, VF breaks the symmetry that one would have expected for $R_b = 0$ and maxima or minima of the same amplitude (see figure 8).

At this stage, the present work should guide future experimental analysis and nonlinear simulations by giving stability trends in parameter space. A full comparison with experiments will be possible only if additional information is obtained on the nonlinear dynamics ensuing the onset of the instability. Further work in this direction is in progress.

Appendix. Supplementary details of the stability at $t_0 = 0$

Figure 15 summarizes the LSA results at $t_0 = 0$ in the (R_b, R_c) plane by showing the stable and unstable regions by unshaded and shaded zones, respectively. The zones I_1, I_2 and I_3 can be shown to correspond respectively to type I dispersion curves, type II dispersion curves and systems where the most unstable growth rate is complex.

The regions I_1 and I_3 lie above the line $R_c = R_L$ and are stable to long-wave instabilities. The neutral stability curve for real growth rates with type I dispersion curves is defined by $R_c = R_S$, where the onset wavenumber is

$$k = \frac{R_b}{3} - \frac{1}{6}\sqrt{R_b^2 + 12D_a}$$

and

$$R_S = R_b + \frac{1}{54D_a}\left(\frac{e^{R_b}+1}{e^{R_b}-1}\right)\left(R_b^3 + \left(R_b^2 + 12D_a\right)^{3/2} + 18R_b D_a\right),$$

which is only defined for $R_b \geqslant 2\sqrt{D_a}$. The point P_1 is defined as the point where $R_c = R_L = R_S$.

The neutral stability curve for complex growth rates is obtained numerically and is defined as $R_c = R_N$ for $R_b \geqslant \lambda\sqrt{D_a}$, where $\lambda \approx 8.3478$. The point P_2 is defined as the point where $R_c = R_S = R_N$. The curve $R_c = R_E$ is numerically obtained and represents the situation when a dispersion curve has two maxima of equal amplitude, with one corresponding to a real growth rate and the other corresponding to a complex growth rate.

Thus, the region I_3 is defined as $R_E < R_c < R_N$, regions I_2 are defined as $(R_L - R_c)R_b > 0$ and the region I_1 lies between $R_L < R_c < \min(R_S, R_E)$. For convenience, the
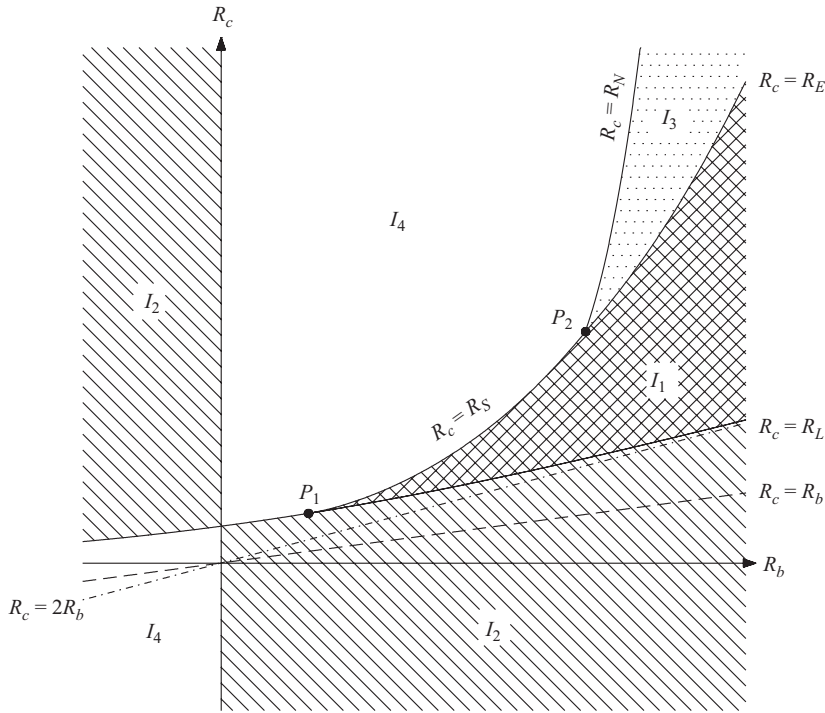
FIGURE 15. A sketch of the various stability regions in the (R_b, R_c) plane at $t_0 = 0$ for $D_a > 0$.

overall neutral stability curve is denoted by R_U which equals R_S for $2\sqrt{D_a} \leqslant R_b \leqslant \lambda\sqrt{D_a}$ and R_N for $R_b > \lambda\sqrt{D_a}$.

REFERENCES

AZAIEZ, J. & SINGH, B. 2002 Stability of miscible displacements of shear thinning fluids in a Hele-Shaw cell. *Phys. Fluids* **14**, 1557.

BÁNSÁGI, T., JR., HORVÁTH, D., TÓTH, A., YANG, J., KALLIADASIS, S. & DE WIT, A. 2003 Density fingering of an exothermic autocatalytic reaction. *Phys. Rev. E* **68**, 55301.

CHADAM, J., HOFF, D., MERINO, E., ORTOLEVA, P. & SEN, A. 1986 Reactive infiltration instabilities. *IMA J. Appl. Math.* **36**, 207.

CROSS, M. & HOHENBERG, P. C. 1993 Pattern-formation outside of equilibrium. *Rev. Mod. Phys.* **65**, 851.

DE WIT, A. 2001 Fingering of chemical fronts in porous media. *Phys. Rev. Lett.* **87**, 054502.

DE WIT, A., BERTHO, Y. & MARTIN, M. 2005 Viscous fingering of miscible slices. *Phys. Fluids* **17**, 054114.

DE WIT, A., DE KEPPER, P., BENYAICH, K., DEWEL, G. & BORCKMANS, P. 2003 Hydrodynamical instability of spatially extended bistable chemical systems. *Chem. Engng Sci.* **58**, 4823.

DE WIT, A. & HOMSY, G. M. 1999a Viscous fingering in reaction–diffusion systems. *J. Chem. Phys.* **110**, 8663.

DE WIT, A. & HOMSY, G. M. 1999b Nonlinear interactions of chemical reactions and viscous fingering in porous media. *Phys. Fluids* **11**, 949.

FERNANDEZ, J. & HOMSY, G. M. 2003 Viscous fingering with chemical reaction: effect of in situ production of surfactants. *J. Fluid Mech.* **480**, 267.

GÁLFI, L. & RÁCZ, Z. 1988 Properties of the reaction front in an $A + B \rightarrow C$ type reaction–diffusion process. *Phys. Rev. A* **38**, 3151.

GÉRARD, T. & DE WIT, A. 2009 Miscible viscous fingering induced by a simple $A + B \rightarrow C$ chemical reaction. *Phys. Rev.* E **79**, 016308.

GHESMAT, K. & AZAIEZ, J. 2009 Miscible displacements of reactive and anisotropic dispersive flows in porous media. *Transport Porous Media* **77**, 489.

HEJAZI, S. H. & AZAIEZ, J. 2010 Non-linear interactions of dynamic reactive interfaces in porous media. *Chem. Engng Sci.* **65**, 938.

HOMSY, G. M. 1987 Viscous fingering in porous media. *Annu. Rev. Fluid Mech.* **19**, 271.

JAHODA, M. & HORNOF, V. 2000 Concentration profiles of reactant in a viscous finger formed during the interfacially reactive immiscible displacements in porous media. *Powder Technol.* **110**, 253.

JIANG, Z. & EBNER, C. 1990 Simulation study of reaction fronts. *Phys. Rev.* A **42**, 7483.

LOGGIA, D., RAKOTOMALALA, N., SALIN, D. & YORTSOS, Y. C. 1995 Evidence of new instability thresholds in miscible displacements in porous media. *Europhys. Lett.* **32**, 633.

LOGGIA, D., SALIN, D. & YORTSOS, Y. C. 1998 The effect of dispersion on the stability of non-monotonic mobility profiles in porous media. *Phys. Fluids* **10**, 747.

MANICKAM, O. & HOMSY, G. M. 1993 Stability of miscible displacements in porous media with nonmonotonic viscosity profiles. *Phys. Fluids* A **5**, 1356.

MISHRA, M., MARTIN, M. & DE WIT, A. 2007 Miscible viscous fingering with linear adsorption on the porous matrix. *Phys. Fluids* **19**, 073101.

MISHRA, M., MARTIN, M. & DE WIT, A. 2008 Differences in miscible viscous fingering of finite width slices with positive or negative log-mobility ratio. *Phys. Rev.* E **78**, 066306.

NAGATSU, Y., BAE, S. K., KATO, Y. & TADA, Y. 2008 Miscible viscous fingering with a chemical reaction involving precipitation. *Phys. Rev.* E **77**, 067302.

NAGATSU, Y., KONDO, Y., KATO, Y. & TADA, Y. 2009 Effects of moderate Damköhler number on miscible viscous fingering involving viscosity decrease due to a chemical reaction. *J. Fluid Mech.* **625**, 97.

NAGATSU, Y., MATSUDA, K., KATO, Y. & TADA, Y. 2007 Experimental study on miscible viscous fingering involving viscosity changes induced by variations in chemical species concentrations due to chemical reactions. *J. Fluid Mech.* **571**, 475.

PANKIEWITZ, C. & MEIBURG, E. 1999 Miscible porous media displacements in the quarter five-spot configuration. Part 3. Non-monotonic viscosity profiles. *J. Fluid Mech.* **388**, 171.

PODGORSKI, T., SOSTARECZ, M. C., ZORMAN, S. & BELMONTE, A. 2007 Fingering instabilities of a reactive micellar interface. *Phys. Rev.* E **76**, 016202.

RONGY, L., TREVELYAN, P. M. J. & DE WIT, A. 2008 Dynamics of $A + B \rightarrow C$ reaction fronts in the presence of buoyancy-driven convection. *Phys. Rev. Lett.* **101**, 084503.

SCHAFROTH, D., GOYAL, N. & MEIBURG, E. 2007 Miscible displacements in Hele-Shaw cells: nonmonotonic viscosity profiles. *Eur. J. Mech.* B **26**, 444.

SWERNATH, S. & PUSHPAVANAM, S. 2007 Viscous fingering in a horizontal flow through a porous medium induced by chemical reactions under isothermal and adiabatic conditions. *J. Chem. Phys.* **127**, 204701.

SWERNATH, S. & PUSHPAVANAM, S. 2008 Instability of a vertical chemical front: effect of viscosity and density varying with concentration. *Phys. Fluids* **20**, 012101.

TAN, C. T. & HOMSY, G. M. 1986 Stability of miscible displacements in porous media: rectilinear flow. *Phys. Fluids* **29**, 3549.

WEI, C. & ORTOLEVA, P. 1990 Reaction front fingering in carbonate-cemented sandstones. *Earth Sci. Rev.* **29**, 183.